ЖЭТФ, 2008, том 133, вып. 4, стр. 805–813

SOLUTIONS OF INDEPENDENT DGLAP EVOLUTION EQUATIONS FOR THE GLUON DISTRIBUTION AND SINGLET STRUCTURE FUNCTIONS IN THE NEXT-TO-LEADING ORDER AT LOW x

G. R. Boroun*

Physics Department, Razi University
67149, Kermanshah, Iran

Received December 18, 2007

We present a set of independent formulas to extract the gluon distribution and the singlet structure function from its derivatives with respect to $\ln Q^2$ in the next-to-leading order of the perturbation theory at low x based on a hard Pomeron exchange. In this approach, both singlet quarks and gluons have the same high-energy behavior at small x. This approach requires the QCD input parameterizations for independent DGLAP evolutions, which we calculated numerically and compared with the MRST, GRV, and DL models. The Pomeron has a hard nature. Its evolution gives a good fit to the experimental data. The obtained values are in the range $10^{-4} \leq x \leq 10^{-2}$ at $Q^2 = 20$ GeV^2.

PACS: 12.38.-t, 12.39.-x, 11.55.Jy

1. INTRODUCTION

The Dokshitzer–Gribov–Lipatov–Altarelli–Parisi (DGLAP) [1] evolution equations are fundamental tools to study the Q^2- and x-evolutions of structure functions, where x is the Bjorken scaling parameter and Q^2 is the squared four-momentum transferred in a deep inelastic scattering process [2]. The measurements of the $F_2(x, Q^2)$ structure function by deep inelastic scattering processes in the small-x region have opened a new era in parton density measurements inside hadrons. The structure function reflects the momentum distributions of the partons in the nucleon. It is also important to know the gluon distribution inside a hadron at low x because gluons are expected to be dominant in this region. The steep increase of $F_2(x, Q^2)$ towards low x observed at the hadron–electron ring accelerator (HERA) also indicates a similar increase in the gluon distribution towards low x in perturbative quantum chromodynamics. In the usual procedure, the deep inelastic scattering data are analyzed by the next-to-leading order QCD fits based on the numerical solution of the DGLAP evolution equations and it is found that the DGLAP analysis can well describe the data in the perturbative region $Q^2 \geq 1$ GeV^2 [3]. As an alternative to the numerical solution, one can study the behavior of quarks and gluons via analytic solutions of the evolution equations. Although exact analytic solutions of the DGLAP equations cannot be obtained in the entire range of x and Q^2, such solutions are possible under certain conditions [4, 5] and are then quite successful as far as the HERA small-x data are concerned.

Small-x behavior of structure functions for fixed Q^2 reflects the high-energy behavior of the virtual Compton scattering total cross section with increasing the total center-of-mass energy squared W^2 because

$$W^2 = Q^2 \left(\frac{1}{x} - 1 \right).$$

The appropriate framework for the theoretical description of this behavior is the Regge-pole exchange picture [6]. It can be asserted with confidence that the Regge theory is one of the most successful approaches to the description of high-energy scattering of hadrons. This high-energy behavior can be described by two contributions: an effective Pomeron with its intercept slightly above unity (∼1.08) and the leading meson Regge trajectories with the intercept $\alpha_R(0) \approx 0.5$ [7].

*E-mail: boroun@razi.ac.ir

The Regge pole model gives the following parameterization of the deep inelastic scattering structure function $F_2(x,Q^2)$ at small x:

$$F_2(x,Q^2)=\sum_i \widetilde{\beta}_i(Q^2)x^{1-\alpha_i(0)}. \tag{1}$$

Here, the singlet part of F_2 is controlled at small x by a Pomeron exchange and the nonsinglet part

$$F_2^{NS}=F_2^p-F_2^n$$

by the A_2 Reggeon [3].

At small x, the dominant role is played by gluons, and the basic dynamic quantity is the unintegrated gluon distribution $f(x,Q_t^2)$, where x denotes the momentum fraction of a parent hadron carried by a gluon and Q_t is its transverse momentum. The unintegrated distribution $f(x,Q_t^2)$ is related to the more familiar scale-dependent gluon distribution $xg(x,Q^2)$ as [4]

$$xg(x,Q^2)=\int^{Q^2}\frac{dQ_t^2}{Q_t^2}f(x,Q_t^2). \tag{2}$$

In the leading $\ln(1/x)$ approximation, the unintegrated distribution $f(x,Q_t^2)$ satisfies the Balitsky–Fadin–Kuraev–Lipatov (BFKL) equation [8]

$$f(x,Q_t^2)=f^0(x,Q_t^2)+\overline{\alpha}_s\times \\ \times\int_x^1\frac{dx'}{x'}\int\frac{d^2q}{\pi q^2}\left[\frac{Q_t^2}{(\mathbf{q}+\mathbf{Q}_t)^2}\times\right. \\ \left.\times\, f(x',(\mathbf{q}+\mathbf{Q}_t)^2)-f(x',Q_t^2)\Theta(Q_t^2-q^2)\right], \tag{3}$$

where

$$\overline{\alpha}_s=\frac{3\alpha_s}{\pi}. \tag{4}$$

This equation gives a sum over the ladder diagrams with a gluon exchange accompanied by virtual corrections that are responsible for the gluon reggeization. In the fixed-coupling case, this equation can be solved analytically and the leading behavior of its solution at small x is given by

$$f(x,Q_t^2)\sim(Q_t^2)^{1/2}\frac{x^{-\lambda_{BFKL}}}{\sqrt{\ln\left(\dfrac{1}{x}\right)}}\times \\ \times\exp\left(-\frac{\ln^2\left(Q_t^2/\overline{Q}^2\right)}{2\lambda''\ln(1/x)}\right), \tag{5}$$

where

$$\lambda_{BFKL}=4\ln(2)\overline{\alpha}_s,\quad \lambda''=\overline{\alpha}_s 28\zeta(3)$$

with the Riemann zeta function $\zeta(3)\approx 1.202$. The parameter $\overline{Q}$ is of a nonperturbative origin.

The quantity $1+\lambda_{BFKL}$ is equal to the intercept of the so-called BFKL Pomeron. Its potentially large magnitude ($\sim$1.5) should be contrasted with the intercept $\alpha_{soft}\approx 1.08$ of the effective soft Pomeron, which has been determined from the phenomenological analysis of the high-energy behavior of hadronic and photoproduction total cross sections. When the model in [7] is used in deep inelastic scattering (specifically, in studying the proton structure functions), a second, "hard", Pomeron (in contrast to the first one called "soft" because of its intercept near 1) must be added, with a larger intercept $\alpha_{hp}\approx 1.4$ [9, 10].

The hypothesis of the Pomeron with the data of the total cross section shows that a better description is achieved in alternative models with the Pomeron having the intercept 1, but with a harder j singularity (a double pole) [11]. This model has two Pomeron components, each of them with the intercept $\alpha_P=1$; one is a double pole and the other is a simple pole [12].

It is tempting, however, to explore the possibility of obtaining approximate analytic solutions of the DGLAP equations themselves in the restricted domain of low x at least. Approximate solutions of the DGLAP equations have been reported [13–15] with considerable phenomenological success. In such an approximate scheme, one uses a Taylor expansion valid at low x and reframes the DGLAP equations as partial differential equations in the variables x and Q^2, which can be solved by standard methods.

In this paper, we suggest approximate analytic independent solutions of the next-to-leading order DGLAP equations for the gluon distribution and the singlet structure function. Therefore, we concentrate on the Pomeron in our calculations, although good fits to the results clearly show that the gluon distribution and the singlet structure function need a model with a hard Pomeron. We compare our results with those from the Gluk–Reya–Vogt (GRV) model [16], Martin–Roberts–Stirling–Thone (MRST) model [17] and Donnachie–Landshoff (DL) fit [10] of parton distributions.

This paper is organized as follows. In Sec. 2, solutions of the DGLAP equations by the Taylor expansion are presented. Section 3 is devoted to the results and discussions.

2. SOLUTION OF THE DGLAP EQUATIONS BY THE TAYLOR EXPANSION

The HERA data should determine the small-x behavior of gluon and singlet quark distributions. We specifically consider the singlet contribution to the proton structure function:

$$F_2^{ep}(x,Q^2) = \frac{5}{18}\Sigma(x,Q^2) + \frac{3}{18}F_2^{NS}(x,Q^2),$$
$$\Sigma(x,Q^2) \equiv x\sum_{i=1}^{N_f}(q_i(x,Q^2)+\overline{q}_i(x,Q^2)), \tag{6}$$

where N_f is the number of active flavors. At small x, the nonsinglet contribution $F_2^{NS}(x,Q^2)$ is negligible and can be ignored. At small x and large Q^2, the singlet quark distribution $\Sigma(x,Q^2)$ is essentially determined by the generic instability of the gluon distribution $xg(x,Q^2)$. To see how this works, we consider the singlet Altarelli–Parisi equations [1], which describe perturbative evolution of $xg(x,Q^2)$ and $\Sigma(x,Q^2)$.

The DGLAP evolution equations for the singlet quark structure function and the gluon distribution have the forms

$$\frac{dG(x,Q^2)}{d\ln Q^2} = \frac{\alpha_s}{2\pi}\times$$
$$\times\int_0^{1-x}dz\left[P_{gg}^{LO+NLO}(1-z)G\left(\frac{x}{1-z},Q^2\right)+\right.$$
$$\left.+\,P_{gq}^{LO+NLO}(1-z)\Sigma\left(\frac{x}{1-z},Q^2\right)\right], \tag{7}$$

$$\frac{d\Sigma(x,Q^2)}{d\ln Q^2} = \frac{\alpha_s}{2\pi}\times$$
$$\times\int_0^{1-x}dz\left[P_{qq}^{LO+NLO}(1-z)\Sigma\left(\frac{x}{1-z},Q^2\right)+\right.$$
$$\left.+\,2n_fP_{qg}^{LO+NLO}(1-z)G\left(\frac{x}{1-z},Q^2\right)\right], \tag{8}$$

where the splitting functions are the leading-order (LO) and next-to-leading order (NLO) Altarelli–Parisi splitting kernels [1, 18]. In the next-to-leading order, the running coupling constant $\alpha_s/2\pi$ is given by

$$\frac{\alpha_s}{2\pi} = \frac{2}{\beta_0 t}\left[1-\frac{\beta_1\ln t}{\beta_0^2 t}\right], \tag{9}$$

where

$$\beta_0 = \frac{1}{3}(33-2N_f), \quad \beta_1 = 102-\frac{38}{3}N_f.$$

The variable t is defined as

$$t = \ln\left(\frac{Q^2}{\Lambda^2}\right)$$

and Λ is the QCD cut-off parameter.

To find an analytic solution, we note that the splitting kernels have the following forms as $z\to 0$ [19]:

$$P_{gg}^{LO+NLO}(z) = \frac{2C_A}{z}+\frac{\alpha_s}{2\pi}\times$$
$$\times\frac{12C_FN_fT_R-46C_AN_fT_R}{9z},$$
$$P_{gq}^{LO+NLO}(z) = \frac{2C_F}{z}+\frac{\alpha_s}{2\pi}\times$$
$$\times\frac{9C_FC_A-40C_FN_fT_R}{z}, \tag{10}$$
$$P_{qq}^{LO+NLO}(z) = \frac{\alpha_s}{2\pi}\frac{40C_FN_fT_R}{9z},$$
$$P_{qg}^{LO+NLO}(z) = \frac{\alpha_s}{2\pi}\frac{40C_AN_fT_R}{9z}.$$

For the $SU(N)$ gauge group, we have

$$C_A = N, \quad C_F = \frac{N^2-1}{2N}, \quad T_F = N_fT_R,, \quad T_R = \frac{1}{2},$$

where C_F and C_A are the color Casimir operators.

We introduce the standard parameterizations of gluon and singlet distribution functions as

$$\Sigma(x,Q^2) = A_Sx^{-\delta_S}(1-x)^{\nu_S}\times$$
$$\times\left(1+\epsilon_S\sqrt{x}+\gamma_Sx\right)\equiv\widetilde{\Sigma}(x,Q^2)x^{-\delta_S},$$
$$G(x,Q^2) = A_gx^{-\delta_g}(1-x)^{\nu_g}\times \tag{11}$$
$$\times\left(1+\epsilon_g\sqrt{x}+\gamma_gx\right)\equiv\widetilde{G}(x,Q^2)x^{-\delta_g},$$

where the usual assumption is that $\delta_{i(=S,g)}=0$. However, the small-x behavior could well be more singular. We note that the behavior of Eqs. (11) with a Q^2-independent value for $\delta_{i(=S,g)}$ obeys the DGLAP equations when $x^{-\delta_{i(=S,g)}}\gg 1$ [4]. According to the Regge theory, the high-energy (low-x) behavior of both gluons and sea quarks is controlled by the same singularity factor in the complex angular momentum plane [6], and we therefore expect $\delta_S=\delta_g=\delta$, where δ is taken as a constant factor throughout the calculation. For the structure functions, we take

$$\widetilde{f}(x,Q^2) = x^\delta f(x,Q^2)$$

to be finite at $x=0$ with δ satisfying $0\le\delta\le$ $\le 1/2$ [20], i.e.,

$$\widetilde{G}(x) = x^\delta G(x), \quad \widetilde{\Sigma}(x) = x^\delta\Sigma(x).$$

Expanding $\widetilde{G}(x/1-z)$ and $\widetilde{\Sigma}(x/1-z)$ about $x=0$, we obtain

$$\begin{aligned}\widetilde{G}\left(\frac{x}{1-z}\right) &= \widetilde{G}(0)+\frac{x}{1-z}\widetilde{G}'(0),\\ \widetilde{\Sigma}\left(\frac{x}{1-z}\right) &= \widetilde{\Sigma}(0)+\frac{x}{1-z}\widetilde{\Sigma}'(0).\end{aligned} \tag{12}$$

The assumptions in these equations are the convergence and the possibility to neglect $O(x^2)$ terms.

Inserting Eqs. (10) and (11) in Eqs. (7) and (8), we obtain the DGLAP equations for the gluon and singlet evolutions at small x:

$$\begin{aligned}\frac{dG}{d\ln Q^2} &= \frac{\alpha_s}{2\pi}\int\limits_0^{1-x} dz\left(\frac{\beta}{1-z}+\frac{\alpha_s}{2\pi}\frac{\gamma}{9(1-z)}\right)\times\\ &\times\left(\frac{x}{1-z}\right)^{-\delta}\times\left[\widetilde{G}(0)+\frac{x}{1-z}\widetilde{G}'(0)\right]+\frac{\alpha_s}{2\pi}\times\\ &\times\int\limits_0^{1-x} dz\left(\frac{\eta}{1-z}+\frac{\alpha_s}{2\pi}\frac{\theta}{9(1-z)}\right)\left(\frac{x}{1-z}\right)^{-\delta}\times\\ &\times\left[\widetilde{\Sigma}(0)+\frac{x}{1-z}\widetilde{\Sigma}'(0)\right]\end{aligned} \tag{13}$$

and

$$\begin{aligned}\frac{d\Sigma}{d\ln Q^2} &= \frac{\alpha_s}{2\pi}\int\limits_0^{1-x} dz\left(\frac{\alpha_s}{2\pi}\frac{\zeta}{9(1-z)}\right)\times\\ &\times\left(\frac{x}{1-z}\right)^{-\delta}\times\left[\widetilde{\Sigma}(0)+\frac{x}{1-z}\widetilde{\Sigma}'(0)\right]+\frac{\alpha_s}{2\pi}\times\\ &\times\int\limits_0^{1-x} dz(2n_f)\left(\frac{\alpha_s}{2\pi}\frac{\xi}{9(1-z)}\right)\left(\frac{x}{1-z}\right)^{-\delta}\times\\ &\times\left[\widetilde{G}(0)+\frac{x}{1-z}\widetilde{G}'(0)\right],\end{aligned} \tag{14}$$

where

$$\begin{aligned}\beta &= 2C_A,\quad \gamma = 12C_FN_fT_R-46C_AN_fT_R,\\ \eta &= 2C_F,\quad \theta = 9C_FC_A-40C_FN_fT_R,\\ \zeta &= 40C_FN_fT_R,\quad \xi = 40C_AN_fT_R.\end{aligned}$$

Solving these equations and taking all the above considerations into account, we find

$$\begin{aligned}&\frac{dG}{d\ln Q^2} =\\ &= U_I\left[\frac{\delta^{\delta-1}}{|\delta-1|^{\delta}}G\left(x\frac{\delta}{|\delta-1|}\right)-\frac{1}{\delta}\widetilde{G}\left(\frac{\delta}{|\delta-1|}\right)\right]+\\ &+U_{II}\left[\frac{\delta^{\delta-1}}{|\delta-1|^{\delta}}\Sigma\left(x\frac{\delta}{|\delta-1|}\right)-\frac{1}{\delta}\widetilde{\Sigma}\left(\frac{\delta}{|\delta-1|}\right)\right],\end{aligned} \tag{15}$$

and

$$\begin{aligned}&\frac{d\Sigma}{d\ln Q^2} =\\ &= V_I\left[\frac{\delta^{\delta-1}}{|\delta-1|^{\delta}}\Sigma\left(x\frac{\delta}{|\delta-1|}\right)-\frac{1}{\delta}\widetilde{\Sigma}\left(\frac{\delta}{|\delta-1|}\right)\right]+\\ &+V_{II}\left[\frac{\delta^{\delta-1}}{|\delta-1|^{\delta}}G\left(x\frac{\delta}{|\delta-1|}\right)-\frac{1}{\delta}\widetilde{G}\left(\frac{\delta}{|\delta-1|}\right)\right],\end{aligned} \tag{16}$$

where

$$\begin{aligned}U_I &= \frac{\alpha_s}{2\pi}\beta+\left(\frac{\alpha_s}{2\pi}\right)^2\frac{\gamma}{9},\quad U_{II} = \frac{\alpha_s}{2\pi}\eta+\left(\frac{\alpha_s}{2\pi}\right)^2\frac{\theta}{9},\\ V_I &= \left(\frac{\alpha_s}{2\pi}\right)^2\frac{\zeta}{9},\quad V_{II} = \left(\frac{\alpha_s}{2\pi}\right)^2(2n_f)\frac{\xi}{9}.\end{aligned}$$

The function $\widetilde{f}(\delta/|\delta-1|)$ $(f=G,\Sigma)$ is a small constant at $x=0$. At small x, this constant can be neglected in Eqs. (15) and (16) due to the singular behavior of the gluon distribution. We therefore have

$$\frac{dG}{d\ln Q^2} = \tau[U_IG(\mu x)+U_{II}\Sigma(\mu x)], \tag{17}$$

and

$$\frac{d\Sigma}{d\ln Q^2} = \tau[V_I\Sigma(\mu x)+V_{II}G(\mu x)], \tag{18}$$

where

$$\tau = \frac{\delta^{\delta-1}}{|\delta-1|^{\delta}},\quad \mu = \frac{\delta}{|\delta-1|}.$$

These equations are a set of formulas to extract the gluon distribution function from the singlet structure function and its derivative $d\Sigma/d\ln Q^2$ and also the singlet structure function from the gluon distribution and its derivative $dG/d\ln Q^2$ at small x in the next-to-leading order of the perturbation theory.

A set of formulas to extract the gluon distribution function from the deep inelastic structure function F_2 and its derivative $dF_2/d\ln Q^2$ at small x in the leading and next-to-leading orders of the perturbation theory was given in [4]. For the specific value $\delta=0.5$ and the number of flavors $N_f=4$, the authors of [4] extracted the gluon distribution with the help of this equation:

$$\begin{aligned}xg(x,Q^2) &= \frac{105}{92e}\frac{1}{\alpha}\frac{1}{1+26.93\alpha}\left[\frac{dF_2(x,Q^2)}{d\ln Q^2}+\right.\\ &\left.+\frac{16}{3}\alpha\left(\frac{107}{60}-2\ln 2\right)F_2(x,Q^2)+O(\alpha^2,x^{1-\delta})\right],\end{aligned} \tag{19}$$

where

$$e=\sum_i^f e_i^2$$

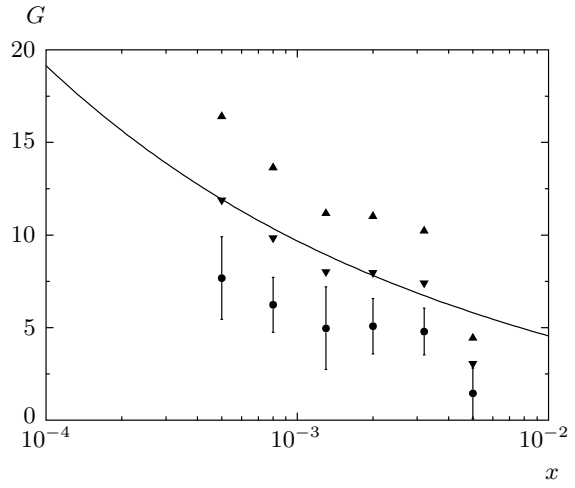

Fig. 1. Our gluon prediction in Eq. (21) using the structure function F_2 and $dF_2/d\ln Q^2$ determined in [21] for a range of x values at $Q^2 = 20$ GeV^2 (solid circles). The error bars show total errors to the H1 data. We compare our results with the KP model [4] (▲), the EKL model [24] (▼), and the MRST fit [17, 22] (solid line)

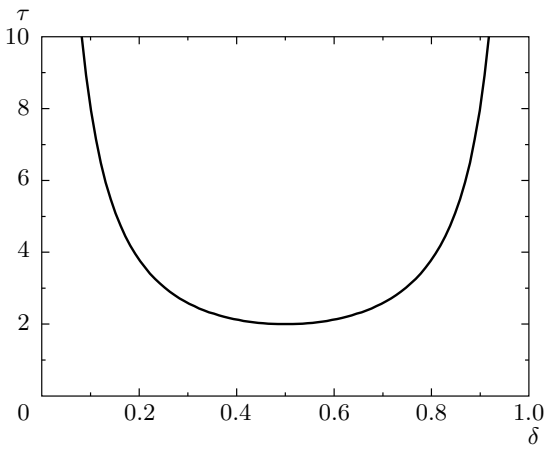

Fig. 2. Behavior of the τ function versus δ values

is the sum of squares of quark charges and

$$\alpha(Q^2) = \frac{\alpha_s(Q^2)}{4\pi}.$$

A different method for determining the gluon distribution at small values of x was proposed in [24] based on the solution of the DGLAP evolution equations in the momentum space up to the next-next-to-leading order. In this method, the quark and gluon momentum densities are assumed to behave as $x^{-\omega_0}$, where ω_0 is a parameter whose actual value must be extracted from the data. Here, the gluon momentum density for four flavors is

$$xg(x,Q^2) = \frac{18/5}{P^{FG}(\omega_0)}\left[\frac{dF_2}{d\ln Q^2} - P^{FF}(\omega_0)F_2\right], \quad (20)$$

where the evolution kernels P^{FG} and P^{FF} calculated in the $\overline{MS}$ scheme are expanded up to third order in α_s.

Using Eq. (18), we can arrive at the gluon distribution function from the F_2 proton structure function and its scaling violation at low x as

$$xg(x,Q^2) = \frac{18}{5V_{II}}\left[\frac{1}{2}\frac{dF_2}{d\ln Q^2} - V_I F_2\right]. \quad (21)$$

By means of these equations, we have extracted the gluon distribution from HERA data using the slopes $dF_2/d\ln Q^2$ determined in [21]. Figure 1 shows the extracted values of the gluon distribution compared to the Kotikov–Parente (KP) model [4], the Ellis–Kunszt–Levin (EKL) model [24], and the MRST fit [17, 22]. This result indicates that our calculations, based on the available structure functions and their derivatives [21], are of the same form as the one predicted by QCD.

In the Regge theory, the high-energy behavior of the hadron–hadron and photon–hadron total cross sections is determined by the Pomeron intercept $\alpha_P = 1+\delta$ and is given by

$$\sigma^{tot}_{\gamma(h)p}(\nu) \sim \nu^{\delta}.$$

This behavior is also valid for a virtual photon for $x \ll 1$, leading to the well-known behavior $F_2 \sim x^{-\delta}$ of the structures at fixed Q^2 and $x \to 0$. The power δ is found to be either $\delta = 0$ or $\delta = 0.5$. The first value corresponds to the soft Pomeron and the second value to the hard (Lipatov) Pomeron intercept. The form $x^{-\delta_g}$ for the gluon parameterization at small x is suggested by Regge behavior, but whereas the conventional Regge exchange is that of the soft Pomeron, with $\delta_g \approx 0.0$, one may also allow a hard Pomeron with $\delta_g \approx 0.5$. The form $x^{-\delta_S}$ in the sea-quark parameterization comes from similar considerations because the process $g \to q\overline{q}$ dominates the evolution of sea quarks at small x. Hence, the fits to early HERA data have the constraint $\delta_S = \delta_g = \delta$, and the value of δ should be close to 0.5 in quite a broad range of small x [4, 9, 10, 25]. Figure 2 illustrates the behavior of the τ function in the kinematic region. The derivative of the τ function is zero at $\delta = 0.5$. For the specific value $\delta = 0.5$, we obtain

$$\frac{dG}{d\ln Q^2} = 2[U_I G(x) + U_{II}\Sigma(x)], \quad (22)$$

and

$$\frac{d\Sigma}{d\ln Q^2} = 2[V_I\Sigma(x) + V_{II}G(x)]. \quad (23)$$

We now discuss how the presented results give the independent evolution equations for the gluon and singlet structure functions at small x. By solving these equations, we find

$$G(x,Q^2) = \frac{1}{2V_{II}}\left[\frac{1}{2}\frac{d}{d\ln Q^2}\left(\frac{1}{U_{II}}\right)\frac{dG(x,Q^2)}{d\ln Q^2} + \right.$$
$$+ \frac{1}{2U_{II}}\frac{d^2G(x,Q^2)}{d\ln^2 Q^2} - \frac{d}{d\ln Q^2}\left(\frac{U_I}{U_{II}}\right)G(x,Q^2) -$$
$$\left. - \frac{U_I}{U_{II}}\frac{dG(x,Q^2)}{d\ln Q^2}\right] -$$
$$- \frac{V_I}{V_{II}}\left[\frac{1}{2U_{II}}\frac{dG(x,Q^2)}{d\ln Q^2} - \frac{U_I}{U_{II}}G(x,Q^2)\right], \quad (24)$$

and

$$\Sigma(x,Q^2) = \frac{1}{2U_{II}}\left[\frac{1}{2}\frac{d}{d\ln Q^2}\left(\frac{1}{V_{II}}\right)\frac{d\Sigma(x,Q^2)}{d\ln Q^2} + \right.$$
$$+ \frac{1}{2V_{II}}\frac{d^2\Sigma(x,Q^2)}{d\ln^2 Q^2} - \frac{d}{d\ln Q^2}\left(\frac{V_I}{V_{II}}\right)\Sigma(x,Q^2) -$$
$$\left. - \frac{V_I}{V_{II}}\frac{d\Sigma(x,Q^2)}{d\ln Q^2}\right] -$$
$$- \frac{U_I}{U_{II}}\left[\frac{1}{2V_{II}}\frac{d\Sigma(x,Q^2)}{d\ln Q^2} - \frac{V_I}{V_{II}}\Sigma(x,Q^2)\right]. \quad (25)$$

Inserting the effective power-law behavior corresponding to Eq. (11) in these equations gives

$$\frac{1}{2V_{II}}\frac{1}{2U_{II}}\frac{d^2\widetilde{G}(Q^2)}{d\ln^2 Q^2} + \left[\frac{1}{2V_{II}}\frac{1}{2}\frac{d}{d\ln Q^2}\left(\frac{1}{U_{II}}\right) - \right.$$
$$- \frac{1}{2V_{II}}\frac{U_I}{U_{II}} - \frac{V_I}{V_{II}}\frac{1}{2U_{II}}\left]\frac{d\widetilde{G}(Q^2)}{d\ln Q^2} + \right[\frac{V_I}{V_{II}}\frac{U_I}{U_{II}} -$$
$$\left. - \frac{1}{2V_{II}}\frac{d}{d\ln Q^2}\left(\frac{U_I}{U_{II}}\right) - 1\right]\widetilde{G}(Q^2) = 0, \quad (26)$$

and

$$\frac{1}{2U_{II}}\frac{1}{2V_{II}}\frac{d^2\widetilde{\Sigma}(Q^2)}{d\ln^2 Q^2} + \left[\frac{1}{2U_{II}}\frac{1}{2}\frac{d}{d\ln Q^2}\left(\frac{1}{V_{II}}\right) - \right.$$
$$- \frac{1}{2U_{II}}\frac{V_I}{V_{II}} - \frac{U_I}{U_{II}}\frac{1}{2V_{II}}\left]\frac{d\widetilde{\Sigma}(Q^2)}{d\ln Q^2} + \right[\frac{V_I}{V_{II}}\frac{U_I}{U_{II}} -$$
$$\left. - \frac{1}{2U_{II}}\frac{d}{d\ln Q^2}\left(\frac{V_I}{V_{II}}\right) - 1\right]\Sigma(Q^2) = 0. \quad (27)$$

These equations show that the structure functions $\widetilde{f}(Q^2)$ are functions of Q^2. The $\ln Q^2$ dependence of $\widetilde{f}(Q^2)$ is observed to be nonlinear [21]. It can be well described by a quadratic expression

$$\widetilde{f}_i(Q^2) = a_i + b_i\ln Q^2 + c_i(\ln Q^2)^2, \quad i = g, \Sigma, \quad (28)$$

where the function $\widetilde{f}(Q^2)$ is determined by the evolution equation resulting from Eqs. (26) and (27) with the starting parameterizations of partons $Q^2 = Q_0^2$ given by the input distributions [10, 16, 17] of the gluon and the singlet and its derivatives, respectively. Therefore, the effective power-law behavior of the gluon distribution and the singlet structure function corresponds to

$$G(x,Q^2) = (a_g + b_g\ln Q^2 + c_g(\ln Q^2)^2)x^{-0.5}, \quad (29)$$

and

$$\Sigma(x,Q^2) = (a_\Sigma + b_\Sigma\ln Q^2 + c_\Sigma(\ln Q^2)^2)x^{-0.5}. \quad (30)$$

3. RESULTS AND DISCUSSION

In this paper, we obtained a new independent evolution descriptions for the gluon distribution and singlet structure function based on Regge-like behavior of distribution functions via Eqs. (24) and (25). In these equations, we need the input functions $F_2(x,Q_0^2)$ and $G(x,Q_0^2)$ and the derivatives of $F_2(x,Q_0^2)$ and $G(x,Q_0^2)$ with respect to $\ln Q^2$ at each constant x value from the QCD parton distributions in the literature [10, 16, 17]. We compared our results of the gluon distribution and singlet structure function in the next-to-leading order with the MRST model [17] and GRV model [16] parameterizations and the DL fit [10]. We have taken the parameterizations fit to the H1 data in [21] with $x < 0.1$ and $2\ \text{GeV}^2 \le Q^2 \le 150\ \text{GeV}^2$. Here, we used the QCD cut-off parameter $\Lambda^4_{\overline{MS}} = 0.323$ GeV [17] for $\alpha_s(M_{z^2}) = 0.119$.

In Figs. 3–5, we show the prediction of Eqs. (26) and (29) for the gluon distribution function. In these calculations, we need $G(x,Q_0^2)$ and its derivative with respect to $\ln Q^2$ at $Q^2 = Q_0^2$. In Fig. 3, we compare our results for the gluon distribution function with the DL fit [10], Martin–Roberts–Stirling (MRSD′_) fit [23], and MRST fit [17]. We have taken the DL parametric form for the starting distribution at $Q_0^2 = 5\ \text{GeV}^2$ given by

$$xg(x,Q^2) = 0.95(Q^2)^{1+\epsilon_0}(1+Q^2/0.5)^{-1-\epsilon_0/2}x^{-\epsilon_0},$$

where ϵ_0 is equal to 0.437 according to a hard Pomeron exchange. As can be seen, the values of the gluon distribution increase as x decreases but its rate of increment is much higher than the MRSD′_ and MRST fits. But

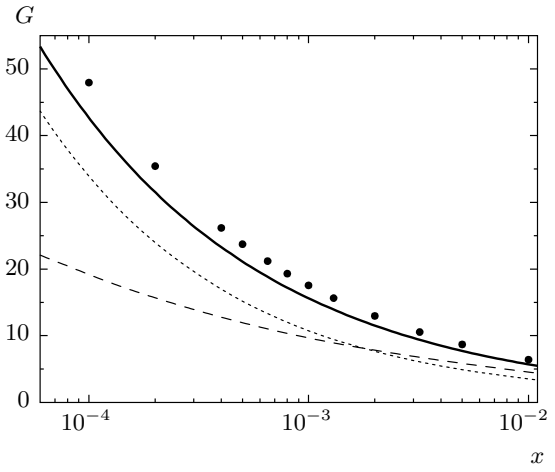

Fig. 3. The gluon distribution given by Eqs. (26) and (29) versus x at fixed $Q^2 = 20$ GeV^2 (solid circles), compared with the DL fit [10] (solid line), the MRSD′_ fit [23] (dotted line), and the MRST fit [17] (dashed line). The starting parameterization of the gluon density at $Q_0^2 = 5$ GeV^2 is given by the DL model

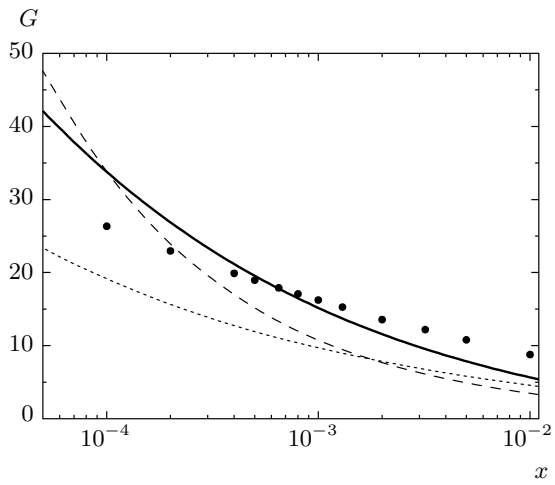

Fig. 4. The gluon distribution given by Eqs. (26) and (29) versus x at fixed $Q^2 = 20$ GeV^2 (solid circles), compared with the next-to-leading-order GRV model [16] (solid line), the MRSD′_ fit [23] (dashed line), and the MRST fit [17] (dotted line). The starting parameterization of the gluon density at $Q_0^2 = 1$ GeV^2 is given by next-to-leading-order GRV model

we do observe that there is some violation at small x. This is because the hard Pomeron exchange defined by the DL model is expected to hold in the small-x limit. One can see that the scaling with the DL fit is nearly preserved in this case.

To better illustrate our calculations at small x, we plot $G(x)$ versus the x variable (see Fig. 4). It can be clearly seen that our results increase as x decreases, but at a somewhat smaller rate. In this figure, we take the next-to-leading-order GRV fit [16] input gluon density at $Q_0^2 = 1$ GeV^2 and compare our results with the GRV fit, MRSD′_ fit [23], and MRST fit [17]. For a constant Q^2, there is a cross-over point for both curves, whose predictions are numerically equal. The cross-over point shifts to MRSD′_ [23] as x decreases. However, we see that this behavior is because our calculations are dependent on the input conditions.

In Fig. 5, we present the gluon distribution $G(x)$ for the H1 HERA proton parameterization at $Q^2 = 20$ GeV^2 [21] for different small-x values. The initial condition for the evolution of the gluon density is assumed to be of the form

$$xg(x,Q_0^2) = 1.1x^{(-0.247)}(1-x)^{17.5}\left(1-4.83\sqrt{x}+68.2x\right)$$

for $Q^2 \geq 3.5$ GeV^2 at the initial scale $Q_0^2 = 4$ GeV^2. The gluon distribution $G(x)$ increases as x decreases. In the same graph, we present the $G(x)$ values for the H1 data [21], MRSD′_ [23], and MRST [17] global fit results; but its rate of increment is higher than that for

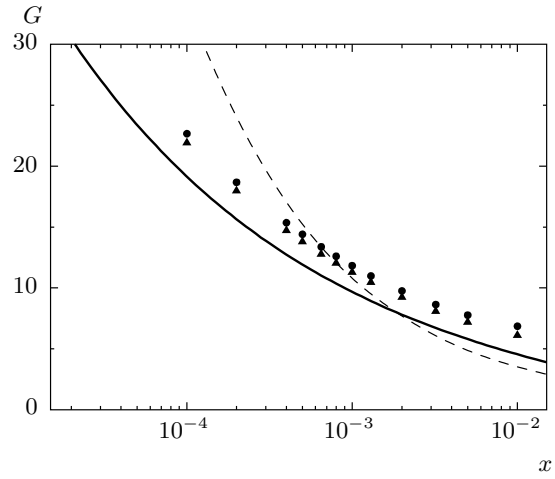

Fig. 5. The gluon distribution given by Eqs. (26) and (29) versus x at fixed $Q^2 = 20$ GeV^2 (solid circles), compared with the H1 data [21] (▲), the MRSD′_ fit [23] (dashed line), and the MRST fit [17] (solid line). The starting parameterization of the gluon density at $Q_0^2 = 4$ GeV^2 is given by the H1 data

the MRST and smaller than for the MRSD′_ data. Our results show that the calculations are sensitive to the initial conditions at $Q^2 = Q_0^2$. For any initial condition, the figures show good agreement between our results and those parameterizations at small x. In this figure,

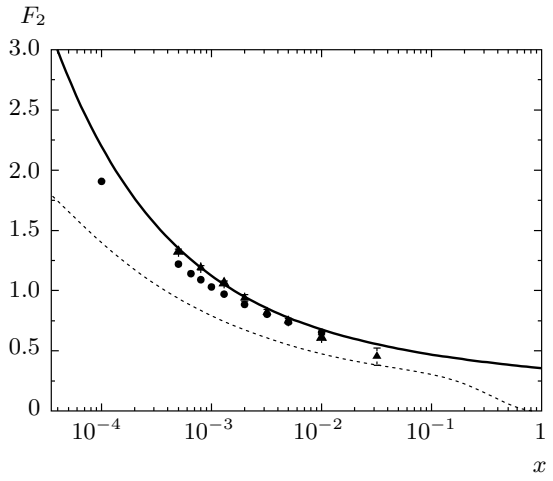

Fig. 6. The calculated values of the singlet structure function $F_2(x,Q^2)$ plotted as functions of x in accordance with Eqs. (27) and (30) with the starting parameterization of the structure function at $Q_0^2 = 5$ GeV^2 given by the DL model (solid circles), compared with the next-to-leading order QCD fit to the H1 data with total errors [21] (▲) and with the DL fit [10] (solid line) and the singlet structure function MRST fit (dotted line)

we show the best fit to the MRST gluon distribution parameterization corresponding to the initial-condition H1 data.

In Fig. 6, we show the prediction of Eqs. (27) and (30) for the singlet structure function. We obtain our results with the input parameterization at the initial scale $Q_0^2 = 5$ GeV^2 and compare with the DL fit [10], MRST fit [17], and H1 data [21] with the total errors at $Q^2 = 20$ GeV^2. In this figure, we observe a continuous increase towards small x. The $\ln Q^2$ dependence of F_2 is observed to be nonlinear. It can be well described by a quadratic expression,

$$\widetilde{\Sigma}(Q^2) = a_S + b_S \ln Q^2 + c_S (\ln Q^2)^2, \qquad (31)$$

which nearly coincides with the QCD fits in the kinematic range of this calculation. Then the effective power-law behavior of the singlet structure function corresponds to

$$F_2(x,Q^2) = \widetilde{F_2}(Q^2) x^{-0.5}. \qquad (32)$$

This behavior is associated with the exchange of an object known as the hard Pomeron. In [9, 10], this behavior was obtained by the simplest fit to the small-x data corresponding to

$$F_2(x,Q^2) = \sum_{i=0,1} f_i(Q^2) x^{-\epsilon_i}, \qquad (33)$$

where the $i = 0$ term is a hard Pomeron exchange and $i = 1$ term is a soft Pomeron exchange. These parameters were obtained from the best fit to all the small-x data for $F_2(x,Q^2)$ together with the data for $\sigma^{\gamma p}$. Hence, our structure function is dominated at small x by the hard Pomeron exchange. This powerful approach to the small-x data for $F_2(x,Q^2)$ is to extend the Regge phenomenology that is so successful for hadronic processes [7]. The Regge theory relates high-energy behavior to singularities in the complex angular momentum plane [6]. Therefore, for deep inelastic scattering, the soft Pomeron contributions is not sufficient to describe the rapid increase with $1/x$ seen in the data at small x and large Q^2. This singularity is a hard Pomeron [9,10].

In conclusion, a set of new formulas connecting the gluon density with its derivative and the singlet structure function with its derivative with respect to $\ln Q^2$ at small x have been presented. We found that the Regge theory can be used to constrain the initial parton densities at $Q^2 = Q_0^2$ and to obtain the distributions at higher virtualities with the DGLAP evolution equations. Careful investigation of our results shows a good agreement with the previously published parton distributions based on QCD. The gluon distribution and singlet structure functions increase as usual, as x decreases. The form of the obtained distribution functions for the gluon distribution and the singlet structure functions are similar to the one predicted from the parton parameterization. The formulas used to generate the parton distributions are in agreement with the increase observed by the H1 experiments. We observed a continuous increase towards small x. The $\ln Q^2$ dependence of $f(x,Q^2)$ is observed to be quadratically nonlinear (see Eq. (28)) which nearly coincides with the QCD fits in the kinematic range of these calculations. Thus, the effective power-law behavior of the parton densities corresponds to

$$f(x,Q^2) = \widetilde{f}(Q^2) x^{-0.5}, \qquad (34)$$

which is associated with an exchange of the object known as the hard Pomeron at small x. The obtained results give strong indications that the proposed formulas, being very simple, provide relatively accurate values for the gluon distribution and structure function.

REFERENCES

1. Yu. L. Dokshitzer, Sov. Phys. JETP **46**, 641 (1977); G. Altarelli and G. Parisi, Nucl. Phys. B **126**, 298

(1997); V. N. Gribov and L. N. Lipatov, Sov. J. Nucl. Phys. **28**, 822 (1978).

2. L. F. Abbott, W. B. Atwood, and A. M. Barnett, Phys. Rev. D **22**, 582 (1980).

3. A. M. Cooper-Sarkar, R. C. E. Devenish, and A. DeRoeck, Int. J. Mod. Phys. A **13**, 3385 (1998).

4. A. K. Kotikov and G. Parente, Phys. Lett. B **379**, 195 (1996); J. Kwiecinski, E-print archives, hep-ph/9607221.

5. R. D. Ball and S. Forte, Phys. Lett. B **335**, 77 (1994); Phys. Lett. B **336**, 77 (1994).

6. P. D. Collins, *An Introduction to Regge Theory and High-Energy Physics*, Cambridge University Press, Cambridge (1997).

7. A. Donnachie and P. V. Landshoff, Phys. Lett. B **296**, 257 (1992).

8. E. A. Kuraev, L. N. Lipatov, and V. S. Fadin, Sov. Phys. JETP **44**, 443 (1976); Sov. Phys. JETP **45**, 199 (1977); Y. Y. Balitsky and L. N. Lipatov, Sov. J. Nucl. Phys. **28**, 1597 (1978).

9. A. Donnachie and P. V. Landshoff, Phys. Lett. B **437**, 408 (1998).

10. A. Donnachie and P. V. Landshoff, Phys. Lett. B **550**, 160 (2002); P. V. Landshoff, E-print archives, hep-ph/0203084.

11. P. Desgrolard, M. Giffon, E. Martynov, and E. Predazzi, Eur. Phys. J. C **18**, 555 (2001).

12. P. Desgrolard, M. Giffon, and E. Martynov, Eur. Phys. J. C **7**, 655 (1999).

13. M. B. Gay Ducati and V. P. B. Gonçalves, Phys. Lett. B **390**, 401 (1997).

14. K. Pretz, Phys. Lett. B **311**, 286 (1993); Phys. Lett. B **332**, 393 (1994).

15. A. V. Kotikov, E-print archives, hep-ph/9507320.

16. M. Gluk, E. Reya, and A. Vogt, Z. Phys. C **67**, 433 (1995); Eur. Phys. J. C **5**, 461 (1998).

17. A. D. Martin, R. G. Roberts, W. J. Stirling, and R. S. Thone, Phys. Lett. B **531**, 216 (2002).

18. W. Furmanski and R. Petronzio, Phys. Lett. B **97**, 437 (1980); Z. Phys. C **11**, 293 (1982).

19. R. K. Ellis, W. J. Stirling, and B. R. Webber, *QCD and Collider Physics*, Cambridge University Press, Cambridge (1996).

20. R. G. Roberts, *The Structure of the Proton*, Cambridge University Press, Cambridge (1990).

21. C. Adloff et al. (H1 Collab.), Eur. Phys. J. C **21**, 33 (2001).

22. A. D. Martin, R. G. Roberts, W. J. Stirling, and R. S. Thone, Eur. Phys. J. C **23**, 73 (2002); A. Vogt, S. Moch, and A. M. Vermasern, Nucl. Phys. B **691**, 129 (2004).

23. A. D. Martin, R. G. Roberts, and W. J. Stirling, Phys. Lett. B **354**, 155 (1995); Phys. Lett. B **306**, 145 (1993).

24. R. K. Ellis, Z. Kunszt, and E. M. Levin, Nucl. Phys. B **420**, 517 (1994).

25. A. D. Martin, M. G. Ryskin, and G. Watt, E-print archives, hep-ph/0406225; J. Kwiecinski and A. M. Stasto, Phys. Rev. D **66**, 014013 (2002).